HHS Public Access

Author manuscript

Sci Transl Med. Author manuscript; available in PMC 2015 August 04.

Published in final edited form as:

Sci Transl Med. 2015 March 18; 7(279): 279ra36. doi:10.1126/scitranslmed.3010755.

MG53-mediated cell membrane repair protects against acute kidney injury

Pu Duann[#1], **Haichang Li**[#1], **Peihui Lin**[1], **Tao Tan**[1], **Zhen Wang**[2], **Ken Chen**[2], **Xinyu Zhou**[1], **Kristyn Gumpper**[1], **Hua Zhu**[1], **Thomas Ludwig**[3], **Peter J. Mohler**[4,5], **Brad Rovin**[5], **William T. Abraham**[5], **Chunyu Zeng**[2], and **Jianjie Ma**[1,3,†]

[1]Department of Surgery, Davis Heart and Lung Research Institute, The Ohio State University, Columbus, OH 43210, USA.

[2]Department of Cardiology, Daping Hospital, The Third Military Medical University, Chongqing Institute of Cardiology, Chongqing 400042, China.

[3]Department of Molecular and Cellular Biochemistry, The Ohio State University, Columbus, OH 43210, USA

[4]Department of Physiology and Cell Biology, Davis Heart and Lung Research Institute, The Ohio State University, Columbus, OH 43210, USA.

[5]Department of Medicine, Davis Heart and Lung Research Institute, The Ohio State University, Columbus, OH 43210, USA.

[#] These authors contributed equally to this work.

Abstract

Injury to the renal proximal tubular epithelium (PTE) represents the underlying consequence of acute kidney injury (AKI) after exposure to various stressors, including nephrotoxins and ischemia/reperfusion (I/R). Although the kidney has the ability to repair itself after mild injury, insufficient repair of PTE cells may trigger inflammatory and fibrotic responses, leading to chronic renal failure. We report that MG53, a member of the TRIM family of proteins, participates in repair of injured PTE cells and protects against the development of AKI. We show that MG53 translocates to acute injury sites on PTE cells and forms a repair patch. Ablation of MG53 leads to defective membrane repair. MG53-deficient mice develop pronounced tubulointerstitial injury and increased susceptibility to I/R-induced AKI compared to wild-type mice. Recombinant human MG53 (rhMG53) protein can target injury sites on PTE cells to facilitate repair after I/R injury or

[†]Corresponding author. jianjie.ma@osumc.edu.

Author contributions: P.D., H.L., B.R., P.J.M., W.T.A., and J.M. developed the concept for the studies. P.D. and H.L. performed I/R- and cisplatin-induced AKI models, tumor allograft animal studies, endogenous MG53 and exogenous rhMG53 characterization, and specimen collections. P.L., T.T., X.Z., K.G., and B.R. performed urinary analyses and biochemical studies. Z.W., K.C., H.Z., and C.Z. performed in vitro cell imaging and toxicological studies of rhMG53. T.L. established KPC-Brca1 tumor cell lines. J.M. oversaw the entire project. P.D., B.R., P.J.M., and J.M. wrote the manuscript, and all authors contributed to revision of the manuscript.

Competing interests: J.M. has an equity interest in TRIM-edicine, which develops rhMG53 for treatment of human diseases. Patents on the use of MG53 are held by Rutgers University–Robert Wood Johnson Medical School.

Citation: P. Duann, H. Li, P. Lin, T. Tan, Z. Wang, K. Chen, X. Zhou, K. Gumpper, H. Zhu, T. Ludwig, P. J. Mohler, B. Rovin, W. T. Abraham, C. Zeng, J. Ma, MG53-mediated cell membrane repair protects against acute kidney injury. *Sci. Transl. Med.* **7**, 279ra36 (2015).

nephrotoxin exposure. Moreover, in animal studies, intravenous delivery of rhMG53 ameliorates cisplatin-induced AKI without affecting the tumor suppressor efficacy of cisplatin. These findings identify MG53 as a vital component of reno-protection, and targeting MG53-mediated repair of PTE cells represents a potential approach to prevention and treatment of AKI.

INTRODUCTION

During normal kidney function, active endocytosis and exocytosis occur in the brush border of the proximal tubular epithelium (PTE) (1, 2). The dynamic membrane trafficking and remodeling processes in PTE cells render them highly vulnerable to membrane injury, necessitating an intrinsic reparative mechanism to support normal renal function and to protect them from excessive damage when exposed to stresses such as ischemia/reperfusion (I/R), nephrotoxins, chemotherapy, or sepsis (3–7). Although the kidney has the ability to repair itself after mild injury, insufficient repair of PTE cells can trigger an inflammatory response causing extensive damage and fibrotic remodeling, leading to progression to chronic renal failure (8–10).

Acute kidney injury (AKI) is commonly encountered in hospital and outpatient settings and is associated with a high rate of mortality. Currently, there are no effective means for preventing or treating AKI. As a result, patients who develop AKI in this setting require lengthy hospital stays, incurring high cost for treatment of AKI and prevention of chronic renal failure. The knowledge gap in understanding the molecular mechanisms associated with repair of injury to PTE cells is a setback in the development of therapies for AKI.

Repair of injury to the plasma membrane is an important aspect of physiology, and disruption of this process can result in pathophysiology in a number of human diseases, including cardiorenal disorders (11–14). We previously identified a TRIM family protein, named MG53, as an essential component of the cell membrane repair machinery (15–19). Redox-dependent oligomerization of MG53 allows for nucleation of intracellular vesicles to the injury site for formation of a membrane repair patch. MG53 knockout mice ($Mg53^{-/-}$) exhibit defective membrane repair in striated muscle that leads to progressive skeletal myopathy and increased vulnerability of cardiomyocytes to I/R-induced injury (15, 16). Although MG53 is predominantly expressed in striated muscles (15, 20), its expression in nonmuscle cells and its physiological role in other organ protection are largely unknown. Our recent study identified an altered form of MG53 expressed in the lung tissue, and intravenous or inhalation delivery of recombinant human MG53 (rhMGS3) protein could ameliorate acute lung injury in rodent models (21).

Here, we show that MG53 constitutes a vital component of reno-protection. We provide data to show that targeting MG53-mediated repair of injury to PTE cells represents a therapeutic approach for prevention of AKI associated with I/R and nephrotoxin exposure. The reno-protective effect of rhMG53 does not appear to interfere with the tumor suppressor function of cisplatin, and thus, rhMG53 can potentially be used to protect renal function during chemotherapy for cancer patients.

RESULTS

MG53 knockout mice exhibit renal pathological phenotypes

Although *Mg53*$^{-/-}$ mice were viable and behaved normally at a young age (until 10 weeks), proteinuria was observed at 20 weeks after birth (Fig. 1A). The *Mg53*$^{-/-}$ mice displayed a higher urine protein–to–urine creatinine ratio (Up/Uc) than did the wild-type littermates under basal conditions (Fig. 1B). Additionally, the serum creatinine (SCr) concentration was significantly elevated in the *Mg53*$^{-/-}$ mice (Fig. 1C) (*P* values and original data are provided in table S1). We also screened the urine of the *Mg53*$^{-/-}$ mice and did not find significant hematuria, leukocyturia, glycosuria, or proteinuria. These data suggest that the *Mg53*$^{-/-}$ mice did not display the typical Fanconi syndrome (22).

Compared with wild-type kidney, the *Mg53*$^{-/-}$ kidney showed pathology at the inner cortex, with pronounced vacuolization and disorganized cisternae (Fig. 1D). Hematoxylin and eosin (H&E) staining showed widening of the interstitial compartment in the *Mg53*$^{-/-}$ kidney (Fig. 1E). On average, the intertubular space was ~2.5-fold larger in the *Mg53*$^{-/-}$ kidney than in the wild-type kidney (Fig. 1G). Transmission electron micrographs revealed disorganized microvilli and brush border at the apical surface of PTE cells derived from the *Mg53*$^{-/-}$ kidney (Fig. 1F), suggesting possible defects in PTE cells.

Pronounced pathologic findings were observed in the junction area between the inner cortex and outer medulla, where PTE cells displayed disorganized mitochondria, abnormal-appearing brush border, and a frequent appearance of vacuoles near the basolateral membrane (fig. S1). These defective structures were observed in ~20% of the PTE cells examined from the *Mg53*$^{-/-}$ mice but rarely seen in the wild-type mouse kidney. After conducting ultrastructural analyses of the *Mg53*$^{-/-}$ glomeruli, we did not find any defects in podocytes such as foot process fusion or glomerular basement membrane detachment (fig. S1). Thus, genetic ablation of *Mg53* led to renal tubulointerstitial defects without affecting glomeruli.

MG53 is expressed in proximal tubule cells and mediates membrane repair

The renal pathology exhibited by the *Mg53*$^{-/-}$ mice led us to investigate whether MG53 is expressed in the kidney. We performed quantitative immunoblotting and found that MG53 was present in the kidney lysates of wild-type mice but not in those of the *Mg53*$^{-/-}$ mice, at a level roughly ~1/40 of the expression in muscle tissues (Fig. 2A). Further tissue fractionation showed that the inner cortex is the main site of MG53 expression, because MG53 was nearly undetectable in the medullary region (Fig. 2A). Using primary cultured PTE cells derived from mice (see fig. S2) and isolated glomeruli and PTE from rats, we found that MG53 was specifically expressed in PTE cells, but not in glomeruli (Fig. 2B). The cell type–specific expression of MG53 was confirmed by immunoblotting with E-cadherin as a PTE marker and nephrin as a glomerular cell marker. We also performed a Western blot with human tissues and found that MG53 could be detected in the kidney but not in the bladder (Fig. 2C).

PTE cells derived from *Mg53*$^{-/-}$ neonates were transfected with GFP-MG53, a fusion construct with green fluorescent protein (GFP) added to the N-terminal end of MG53, to

investigate the extent of MG53's participation in the repair of membrane injury. As shown in Fig. 2D, GFP-MG53 in PTE cells localized to the cytosol, intracellular vesicles, and plasma membrane, a subcellular distribution similar to that observed in striated muscles (15). In response to injury caused by penetration of a microelectrode into the plasma membrane, GFP-MG53 rapidly translocated toward the acute injury site (Fig. 2D). This GFP-MG53 translocation to membrane injury sites in PTE cells is similar to that observed in C2C12, human embryonic kidney (HEK) 293, and other cell types (15, 17).

MG53-mediated cell membrane repair could also be recapitulated in human PTE cells. HKC-8 cells, an immortalized human renal proximal tubular cell line established by Racusen *et al*. (23), are widely used as a model system for kidney research. With HKC-8 cells, we found that GFP-MG53 moved to sites of acute injury induced by mechanical perturbation of the plasma membrane (fig. S3 and movie S1). Furthermore, transfected GFP-C242A, a mutant form of MG53 that cannot oligomerize in response to environmental redox changes after acute cellular injury (15), failed to form a repair patch in mechanically injured HKC-8 cells (movie S2). These studies recapitulate in human kidney cells our mouse data showing that MG53 facilitates nucleation of membrane repair machinery in a redox-dependent fashion after acute cellular injury.

A striking phenomenon was observed when we compared the susceptibility of PTE cells derived from wild-type and *Mg53*$^{-/-}$ mice to mechanical injury. As shown in Fig. 2E, wild-type PTE cells were able to survive microelectrode penetration (top), whereas *Mg53*$^{-/-}$ PTE cells always died within 10 s of injury (bottom). On average, ~93% of wild-type cells survived, but all the *Mg53*$^{-/-}$ cells rapidly died. This outcome reflected defective membrane repair capacity, because restoration of MG53 by gene transfection increased survival of the *Mg53*$^{-/-}$ PTE cells (Fig. 2F). The striking difference in response of wild-type and *Mg53*$^{-/-}$ PTE cells after mechanical injuries could be visualized in movies S3 and S4.

Another interesting observation was related to changes in morphology of the *Mg53*$^{-/-}$ PTE cells examined under scanning electron microscopy. As shown in fig. S4, PTE cells derived from wild-type mice show characteristic microvilli at the apical surface and filopodia that extend from the plasma membrane (fig. S4, A and B), whereas the *Mg53*$^{-/-}$ PTE cells show fewer microvilli and disorganized filopodial structures (fig. S4, C and D).

Mg53$^{-/-}$ mice exhibit exacerbated kidney injury under I/R

To test if MG53-mediated repair of injury to PTE cells contributes to maintenance of renal function under physiologic and pathophysiologic conditions, we compared the response of the *Mg53*$^{-/-}$ mice and wild-type littermates to I/R-induced AKI (Fig. 3). H&E and PAS (periodic acid–Schiff) staining revealed that *Mg53*$^{-/-}$ mice develop kidney pathology under basal conditions (sham operation with mice at 11 weeks of age) (Fig. 3B). Animals subjected to I/R injury to the kidney (25-min ischemia) showed exaggerated tubular injury, as demonstrated by the increase in hyaline casts in tubular lumens and loss of nuclei, suggestive of acute tubular necrosis (ATN) (Fig. 3B). The Up/Uc ratio was increased in the *Mg53*$^{-/-}$ mice at each time point after I/R injury to the kidney (Fig. 3C), and SCr measurements showed compromised kidney function at 5 days after I/R injury (Fig. 3D). In summary, the *Mg53*$^{-/-}$ kidney showed widening of intertubular spaces under basal

conditions (with sham surgery), and I/R treatment led to exacerbation of ATN phenotypes. These data show that MG53 deficiency leads to aggravation of I/R-induced AKI.

rhMG53 protein recognizes injury sites on PTE cells to facilitate reno-protection

We previously showed that rhMG53 protein protects various cell types against cell membrane disruption when applied to the extracellular environment (17). Moreover, administration of rhMG53 provided dose-dependent protection against injury to muscle cells and ameliorated the pathology associated with muscle dystrophy (17). The association of rhMG53 with sites of membrane disruption requires recognition of lipid-based signals, and our previous findings indicated that MG53 can bind phosphatidylserine (PS) (17), a phospholipid usually sequestered in the inner leaflet of the plasma membrane that may be exposed to the extracellular environment after injury. Therefore, the association of rhMG53 with exposed PS at the tissue injury site might provide an anchoring mechanism for the tissue-protective function of rhMG53.

When rhMG53 was applied to cultured renal epithelial cells, it targeted acute injury sites on the cell membrane and facilitated repair of membrane damage in response to anoxia/reoxygenation (A/R). As shown in Fig. 4, co-localization of rhMG53 and annexin V at the plasma membraneof PTE cells was observed after A/R injury (Fig. 4, bottom panels). Uninjured PTE cells were negative for staining with rhMG53 or annexin V (Fig. 4, top panels). PTE cells incubated with BSA as a control showed neither plasma membrane targeting nor intracellular localization of BSA (Fig. 4, middle panels).

rhMG53 protects animals from I/R-induced AKI

On the basis of studies with the cultured renal epithelial cells, we tested whether rhMG53 was effective in protection against I/R-induced AKI in animal models. We first used a semiquantitative immunoblotting method to investigate the glomerular permeability of rhMG53 and its ability to reach PTE cells in healthy Sprague-Dawley rats (fig. S5A). Various amounts of rhMG53 were administered to rats through tail vein injection, and excretion of rhMG53 into urine was measured at 1.5 to 6 hours after intravenous administration. rhMG53 could be detected in the urine, suggesting that healthy glomeruli are permeable to rhMG53. For I/R-induced AKI, rats were subjected to 35 min of ischemia to the left kidney with a non-occlusive vessel clamp on the renal pedicle and contralateral nephrectomy. Two doses of rhMG53 (2 mg/kg) were applied intravenously, one before renal artery clamping and one after release of renal artery clamping. By immunohistochemistry (IHC), anti-MG53 antibody detected rhMG53 distribution in a discrete peri-lumen tubular pattern at 2 hours after I/R-induced kidney injury (fig. S5B). rhMG53 staining was undetectable in kidneys from BSA-treated or sham-operated rats. These results suggest that I/R induces recruitment of rhMG53 to the injured renal epithelia.

Reduced albuminuria (Ualb/Uc) was observed in rhMG53-treated rats when compared with the vehicle-treated group at different times after I/R injury (Fig. 5A). SCr was also reduced in rats that received rhMG53 treatment (Fig. 5B). Kidney injury molecule–1 (KIM-1) is a PS receptor expressed on renal PTE cells that has been widely used as a biomarker for kidney injury (24, 25). IHC staining for KIM-1 revealed that intravenous administration of rhMG53

reduced KIM-1–positive PTE cells at 5 days after I/R-induced kidney injury when compared with vehicle-treated controls (Fig. 5C). rhMG53-mediated improve ment in kidney pathology was also evident in histopathology analysis of H&E staining (Fig. 5D). On the basis of KIM-1 staining (Fig. 5C), we quantified the degree of tubular injury in Fig. 5E, confirming that the administration of rhMG53 ameliorates I/R-induced AKI in the rats. There was no apparent toxicity from rhMG53, as revealed by the healthy kidneys of the rhMG53-treated uninjured rats (Fig. 5, C and D). Together, these results support the reno-protective effect of rhMG53 against the development of I/R-induced AKI.

rhMG53 protects animals from cisplatin-induced AKI without affecting its antitumor function

To test if rhMG53-PS interaction contributes to the reno-protective effect of MG53 in AKI, we used nephrotoxin-induced AKI as another animal model. Cisplatin is a widely used chemotherapeutic reagent for treatment of cancers, and it is also known as a nephrotoxin because of its detrimental effect on kidney function in cancer patients (26, 27). Although the mechanism of action for cisplatin in tumor suppression involves intercalation and disruption of DNA-synthesizing activities (4, 28), several studies have shown that a high-affinity interaction between PS and cisplatin appears to contribute to certain aspects of its nephrotoxicity (29, 30). Cisplatin-induced perturbation of PS distribution may share some common features with I/R-induced injury to the cell membrane, where increased oxidative stress and lipid peroxidation may lead to breakdown of the plasma membrane and appearance of PS at the extracellular space (31). Using cultured PTE cells, we found that treatment with cisplatin led to exposure of PS at the cell surface membrane, as evidenced by immunostaining with FITC–annexin V. In addition, colocalization of rhMG53 and annexin V could be observed at the cisplatin-induced injury sites on PTE cells (Fig. 6). Whereas control PTE cells are negative for staining with rhMG53 or annexin V (Fig. 6, top panels), cells exposed to cisplatin showed positive staining with rhMG53 and annexin V (Fig. 6, bottom panels). In addition to localization at the plasma membrane (overlapping pattern with annexin V), rhMG53 also enters the PTE cells after exposure to cisplatin. Cells incubated with BSA showed neither plasma membrane targeting nor intracellular localization of BSA after cisplatin treatment (Fig. 6, middle panels). These data support the concept that PS functions as an important lipid signal for the tissue-protective function of rhMG53.

We followed a well-established protocol of murine nephrotoxin-induced AKI (32) and treated C57BL/6 mice with cisplatin (30 mg/kg) via intraperitoneal injection. This treatment led to the development of AKI, as evidenced by the appearance of pathological features of ATN in cisplatin-treated animals (Fig. 7A). To test if rhMG53 can protect against cisplatin-induced AKI, the animals were treated with intravenous injection of rhMG53 10 min before intraperitoneal delivery of cisplatin. As shown in Fig. 7 (B and C), improvements in Up/Uc and SCr were observed in animals that received rhMG53 treatment, indicating that rhMG53 is effective in preventing the nephrotoxic effect of cisplatin. These results support targeting repair of PTE injury as a potential mechanism for alleviating the nephrotoxic effect of cisplatin.

To assess whether rhMG53 interferes with the efficacy of cisplatin to induce death in cancer cells, we performed the following two studies. Using cultured murine pancreatic tumor cells (KPC-Brca1) (33, 34) in an MTT [3-(4,5-dimethylthiazol-2-yl)-2,5-diphenyltetrazolium bromide] assay, we found that incubation with rhMG53 (50 μg/ml) did not affect the median inhibitory concentration (IC_{50}) of cisplatin-induced cancer cell death at 48 hours after drug treatment (Fig. 7D). We then used a pancreatic cancer allograft model to test if co-injection of rhMG53 alters the tumor suppression function of cisplatin. As shown in Fig. 7E, cisplatin (6 mg/kg, intraperitoneal) effectively suppressed growth of KPC-Brca1 tumor cells implanted into nude mice. There was no difference in the pattern of tumor growth in animals receiving cotreatment with rhMG53 and cisplatin. Thus, the reno-protective function of rhMG53 did not appear to interfere with the efficacy of cisplatin to treat tumor cells.

Repetitive intravenous administration of rhMG53 does not produce adverse effects in dogs

To determine the pharmacokinetic properties and evaluate the safety profile of rhMG53 in a large animal model, we conducted repeated intravenous administration of rhMG53 in beagle dogs. The dogs received a total of seven doses of rhMG53 (1 mg/kg body weight). As shown in Fig. 8A, histological analyses did not reveal gross abnormalities within major vital organs, including heart, lung, kidney, liver, brain, and spleen, indicating that the animals could tolerate repetitive exposure to rhMG53. Measuring the serum concentration of rhMG53 by enzyme-linked immunosorbent assay (ELISA) showed that the pharmacokinetic properties of MG53 remained unchanged from the beginning (first dose) to the end of repeated intravenous administration (seventh dose), with a half-lifetime of ~1.4 hours at both time points (Fig. 8B), which is similar to its half-lifetime in mice (17). The rapid clearance of rhMG53 in both rodents and dogs indicates that renal excretion of rhMG53 via glomerular filtration occurs under normal physiological conditions and that rhMG53 can be delivered to the desired site of therapeutic action, the proximal tubule.

DISCUSSION

Our data present evidence that MG53-mediated membrane repair constitutes a vital component of reno-protection under both physiological and pathophysiological conditions. Defects in membrane repair due to the absence of MG53 can lead to increased susceptibility of the kidney to stress-induced injury. We show that MG53 is expressed in the renal proximal tubule and that PTE cells derived from the $Mg53^{-/-}$ kidney are defective in repair of acute membrane injury. Ultrastructural analyses reveal that the prominent defects with the $Mg53^{-/-}$ kidney reside within the apical surface of PTE cells, where active endocytosis and exocytosis occur under normal physiological conditions. Thus, targeting MG53-mediated repair of injury to PTE cells represents a therapeutic approach for prevention of AKI associated with I/R and nephrotoxin exposure.

The proximal tubule, especially the S3 segment, is the most affected nephron segment during ischemia or nephrotoxin insult (35). We find that MG53 expression is enriched in the inner cortex but not present in the medulla region, further supporting the physiological function for MG53 in protection against injury to the kidney. MG53 has a molecular size of 53 kD and contains positive charges (isoelectric point = 6.2) (15). Previous studies showed

that proteins with comparable properties can cross the glomerulus (36, 37), thus suggesting that intravenously administered rhMG53 could access the apical surface of PTE cells. Indeed, we have shown that rhMG53 can be excreted into the urine within a few hours after intravenous administration, in a time frame consistent with the pharmacokinetic properties of rhMG53 in the serum (17). Because the amount of MG53 in the urine did not increase proportionally to the amount of the injected rhMG53, it is possible that MG53 secreted from PTE cells could also contribute to the appearance of MG53 in the urine. MG53 from either filtration or secretion could help to repair the injury of tubular epithelial cells. We find that rhMG53 can target the injured PTE cells, but not PTE cells in healthy kidneys. This sug gests that injury to the kidney provides a means for rhMG53 to access the apical surface of the renal epithelium. Stress-induced injury to the kidney, caused by either I/R or cisplatin, leads to exposure of PS at the apical surface of PTE cells, which serves as an anchoring mechanism for rhMG53 to initiate the repair process for AKI.

Our data support a potential role for rhMG53 in human AKI. Our study with rhMG53 in the prevention of cisplatin-induced renal toxicity is particularly exciting, because it represents a therapeutic agent that can selectively protect kidney function without interfering with the tumor suppressor efficacy of cisplatin. The mechanism of cisplatin in tumor suppression involves blocking DNA synthesis, and there is no evidence to suggest that rhMG53 participates in this process, allowing rhMG53 to be used as a potential adjuvant for chemotherapy to bypass the nephrotoxicity of cisplatin. In addition to nephrotoxin-induced kidney injury, cardiothoracic surgery–associated AKI is also a major clinical problem, because about one-third of the patients undergoing this type of surgery develop AKI (6, 38). We showed that intravenous delivery of rhMG53 before ischemia and reperfusion is effective in preventing the onset of AKI in rodent models. Prophylactic administration of rhMG53 to patients before cardiothoracic surgery or nephrotoxic chemotherapy would be a potential strategy for prevention of AKI and associated complications. Because MG53 is present in the circulation under normal physiologic conditions (17), the administration of rhMG53 should not produce an immune response and would potentially be a safe biologic reagent for treatment of acute tissue injuries.

Since our discovery of MG53 in 2009 (15, 18, 39), notable progress has been made in advancing the mechanistic action of this gene in the biology of tissue repair and also in regulation of metabolic syndromes. MG53 belongs to the TRIM family of proteins that contain the conserved RING motif with E3 ligase activity. Several studies have shown that insulin receptor substrate–1 (IRS-1) (20, 40) and focal adhesion kinase (FAK) (41) are E3 ligase substrates for MG53-mediated ubiquitination and degradation. A recent report by Song *et al*. (40) stated that MG53 expression is markedly elevated in animal models of insulin resistance and that MG53 overexpression suffices to trigger muscle insulin resistance and metabolic syndrome. However, a separate report by Yi *et al*. (20) presented no evidence for MG53 up-regulation in diabetes, and muscle samples derived from human diabetic patients and mice with insulin resistance showed normal expression of MG53, indicating that altered MG53 expression does not serve as a causative factor for the development of metabolic syndrome. The observation that MG53 expression remains unchanged in metabolic syndromes was also presented in early studies by other investigators (42–44).

Although MG53-mediated down-regulation of IRS-1 could contribute to the dys-regulation of glucose metabolism in skeletal muscle, early publications by Tamemoto *et al*. (45) and Terauchi *et al*. (46) showed that animal models with knockout of IRS-1 show normal glucose tolerance compared with wild-type control mice. This further challenges the proposal by Song *et al*. (40) that MG53-mediated down-regulation of IRS-1 serves as a causative factor for the development of metabolic syndromes. Clearly, more studies are required to dissect the functional relationship between MG53 and IRS-1 in regulation of metabolic function, because this is fundamental for our effort to translate the basic findings into clinical application. In principle, protein engineering of MG53 that disrupts the putative E3 ligase activity without affecting its membrane repair function may offer a better approach for rhMG53 in treatment of AKI and chronic renal diseases.

A limitation of our study is that the in vivo tests of protection against AKI with rhMG53 were all conducted in rodent models. Notable differences exist in the anatomy and function of the kidneys between rodents and large animals. Although repetitive intravenous doses of rhMG53 produced no adverse effects in rodents and dogs, suggesting that rhMG53 may be well tolerated in human studies, further determining the efficacy of rhMG53 in protection against AKI in large animal models will be required before initiation of clinical studies in human subjects. In addition, rhMG53 used in the present study was produced from *Escherichia coli* fermentation, which may not be optimal for use as an injectable protein therapeutic agent. Future studies may explore the use of mammalian cell expression systems, such as Chinese hamster ovary cells, for generation of rhMG53 protein for human studies. Establishing the proper protocol to allow for large-scale production of rhMG53 in mammalian cells can have an advantage over the current prokaryotic expression system.

Many additional studies will be necessary to achieve complete understanding of the molecular mechanisms of repair of injury to PTE cells. In addition to MG53, other genes, such as dysferlin (14), caveolin 3 (18), annexin (47), NM-IIA (48), and PTRF (49), may also participate in the assembly of the cell membrane repair machinery. It will also be necessary to assess whether genetic variations in MG53 expression or its associated repair machinery predispose patients to ischemic or nephrotoxic kidney injury. If so, this could provide a way to screen patients to determine their susceptibility to AKI before treatments that may cause AKI.

MATERIALS AND METHODS

Study design

The main goal of this study was to explore the potential of targeting the intrinsic cell membrane repair machinery in treatment of AKI. Wild-type and $Mg53^{-/-}$ littermate mice were used to examine their susceptibility to I/R-induced AKI. The efficacy of the rhMG53 protein for protection against AKI was evaluated after intravenous administration of rhMG53 in animal models of I/R- or nephrotoxin-induced AKI. A sample size of at least six animals per group was used for all experimentation. All analyses were performed blinded to genotype and/or treatment.

Reagents, human tissue specimens, and cells

rhMG53 protein was purified from *E. coli* following our published protocol (17). rhMG53 was stored as lyophilized powder and dissolved in saline solution before use. Anti–E-cadherin antibody was purchased from Proteintech Group, anti–KIM-1 antibody was obtained from R&D Systems, anti-nephrin antibody was from Santa Cruz Biotechnology, and anti–β-actin was from Sigma. FITC–annexin V was purchased from BD Biosciences. Human kidney and bladder tissues were obtained from National Disease Research Interchange Biospecimen. Immortalized PTE cells from WKY rats were cultured as described before (50, 51).

Animal care and procedures

Animal handling and surgical procedures were performed according to protocols approved by the Institutional Animal Care and Use Committee (IACUC) of The Ohio State University and were compliant with guidelines of the American Association for the Accreditation of Laboratory Animal Care. MG53 knockout mice ($Mg53^{-/-}$) and their wild-type control mice were bred and maintained as previously described (15). Sprague-Dawley rats (weighing 250 to 300 g) were purchased from Charles River. NCR nude mice (3 to 5 weeks of age) were purchased from Taconic Farms. Male beagle dogs (8 to 11 kg) were purchased from Marshall BioResources.

Mouse model of I/R-induced AKI—Mice (10 to 14 weeks of age) were anesthetized with isoflurane. The left renal pedicle was exposed using a dorsal lumbotomy incision, and the left renal artery was subjected to unilateral non-occlusive clamping for 25 min at room temperature, followed by reperfusion, which was ensured by visual inspection of the kidneys. Sham-operated animals had an incision plus 30 min of waiting time without clamping. After ischemia or sham surgery, flank muscle and skin layers were sutured, and 1 ml of prewarmed 0.9% saline solution was subcutaneously administered immediately before closing the incision to prevent dehydration.

Rat model of I/R-induced AKI—Rat kidneys were approached through a ventral midline incision. The left renal pedicle was clamped by a non-occlusive vascular clip, followed by contralateral nephrectomy. The left renal artery was released for reperfusion after 35 min of ischemia, and the kidney was visually checked for color changes. Sham-operated rats received a ventral midline incision and suture without I/R of the kidney. To test whether rhMG53 could prevent I/R-induced AKI in the rat model, rhMG53 (2 mg/kg) was tail vein–administered 10 min before ischemia and 5 min before reperfusion. Control animals received an equal volume of saline solution during the I/R procedure.

Mouse model of cisplatin-induced AKI—Mice were treated with cisplatin (30 mg/kg) (a solution of 1.0 mg/ml in sterile 0.9% saline) or vehicle (0.9% saline) by a single intraperitoneal injection. After cisplatin administration, mice were placed in metabolic cages for three successive days for urine sample collection. rhMG53 (2 mg/kg) was delivered through tail vein injection at 10 min before cisplatin administration (intraperitoneal). Kidneys were harvested at the completion of urine collection, bisected, and fixed in 10% neutral buffered formalin for IHC.

Measurement of renal function

Urine samples were collected by housing the animals in metabolic cages for 18 to 20 hours with free access to water and food. For detection of possible hematuria, leukocyturia, and glycosuria, urine samples were spotted onto 10SG urine reagent strips (McKesson Medical-Surgical) and read on a Siemens CLINITEK Status Analyzer (Siemens Healthcare Diagnostics). The CLINITEK was calibrated before use and ran a self-check before each urine sample was read. All urines were read on the same day and by the same operator to ensure consistency. Semiquantitative urine parameters (protein, pH, specific gravity, and glucose) were averaged for each mouse within a group, and then group averages for wild-type and $Mg53^{-/-}$ mice were determined. None of the mice tested positive for urine leukocytes, and only one mutant and one wild-type mouse had blood in their urines, but even these two mice did not have blood in every urine sample collected over several days. Urinary protein excretion was measured by the Bradford method using a Bio-Rad DC protein determination kit and SDS-PAGE, followed by colloidal blue staining. Uc was measured by the Jaffe method using a BioQuant kit (BQ Kits Inc.). Urine albumin concentration was quantified using an ELISA kit (Bethyl Laboratories).

Blood chemistry

Blood samples were obtained by cardiac puncture technique at the time when mice were euthanized. SCr levels were measured by a high-performance liquid chromatography–based method at the Yale University Mouse Metabolic Phenotyping Center Analytic Core.

Immunoblotting

Crude extracts from dissected cortical or medullary regions of the mouse kidney were washed twice with ice-cold phsophate-buffered saline (PBS) and lysed in radioimmunoprecipitation assay buffer [10 mM tris-HCl (pH 7.2), 150 mM NaCl, 1% NP-40, 0.5% SDS, and 0.5% deoxycholate], supplemented with a cocktail of protease inhibitors (Sigma) and phosphatase inhibitors (Thermo Scientific). Kidney lysates (50 μg) were separated by 10% SDS-PAGE and transferred onto polyvinylidene difluoride membranes (Millipore). The blots were washed with tris-buffered saline–Tween 20 (TBST), blocked with 5% milk in TBST for 1 hour, and incubated with custom-made monoclonal anti-MG53 antibody (15, 17, 21). Immunoblots were visualized with an ECL Plus kit (Pierce).

For assaying cell type–specific expression of MG53 in kidney, PTEs and glomeruli were isolated from adult rat kidney using the method of differential sieving (52). Identities of cell origins were confirmed with E-cadherin as a PTE cell marker and nephrin as a glomerular cell marker.

Primary PTE cell isolation from mouse neonates

Primary PTE cells were isolated from kidneys of 2-day-old $Mg53^{-/-}$ neonates and wild-type littermates using the protocol of Lieberthal *et al*. with minor modification (53). In brief, kidney cortices from mice were retrieved under a dissecting microscope, minced and digested with collagenase for 30 min at 37°C, and filtered through a 70-μm sieve over a 50-

ml conicaltube with medium containing Dulbecco's modified Eagle's medium (DMEM) and Ham's F-12 (1:1 ratio) supplemented with transferrin (5 μg/ml), insulin (5 μg/ml), and hydrocortisone (50 μM). The filtered cells were centrifuged and plated onto a Matrigel-coated plate (BD Biosciences) and cultured for 3 days before experimentation. Aliquots of cells were stained with phaseolus erythroagglutinin (Pha-E) lectin (Sigma-Aldrich) to confirm identity of PTEs (see fig. S2).

Transfection of GFP-MG53 into PTE cells derived from the $Mg53^{-/-}$ neonates was performed using the Lipofectamine LTX Reagent (Life Technologies) per the manufacturer's instructions. PTE cells expressing GFP-MG53 were subjected to microelectrode penetration–induced acute injury to the plasma membrane as previously described (15).

Electron microscopy

Electron microscopy was performed by the Ohio State University Campus Microscopy and Imaging Facility (CMIF). Renal tissues were sliced in blocks of 1-mm cubes and fixed at room temperature with a fixative solution containing 2.5% glutaraldehyde, 1% formaldehyde, and 100 mM sodium phosphate (pH 7.2). These slices were rinsed with 0.1 M Na cacodylate (pH 7.4) and postfixed for 1 hour in 2% osmium tetroxide. After dehydration, the samples were embedded in epoxy resin, and ultrathin sections (60 nm) were counterstained with uranyl acetate and lead citrate. Transmission electron microscopy images were obtained with an FEI Tecnai G2 Spirit Transmission Electron Microscope (FEI Hillsboro) equipped with a MacroFire MonoChrome progressive scan charge-coupled device camera (Optronics). Sections of PTE and glomeruli pathology were analyzed.

Scanning electron microscopic images of PTE cells were used to analyze the morphological changes of the cells derived from wild-type and $Mg53^{-/-}$ mice. Cells grown on Matrigel-coated glass coverslips were fixed with 2% paraformaldehyde and 2.5% glutaraldehyde in 0.1 M sodium cacodylate and then postfixed in 1% osmium tetroxide for 1 hour. After dehydration, the cells were sputter-coated with palladium and viewed under an FEI Nova NanoSEM 400 scanning electron microscope (FEI).

Histopathology and IHC staining

Experimental animals were euthanized 2 hours after tail vein injection of rhMG53. Systemic perfusion of the animals was immediately conducted with heparin-supplemented PBS (pH 7.4, 200 ml), followed by 2% paraformaldehyde in 200 ml of PBS using a peristaltic infusion pump (50 ml/min). Kidneys were harvested, embedded in O.C.T. Tissue-Tek medium (Sakura), and snap-frozen by immersion in an isopentane bath at −80°C. Cryosections (6 μm thick) were mounted on Superfrost Plus microscope slides (Fisher Scientific) and fixed in freshly prepared 4% paraformaldehyde in PBS at 4°C. Immunostaining was carried out using a custom-made rabbit anti-human MG53 antibody (15, 17, 21). Alexa 488–conjugated sheep anti-rabbit immunoglobulin G (Molecular Probes) was used for labeling of kidney sections that were positive for rhMG53 staining, using a digital fluorescence microscope.

Paraffin-embedded kidney sections of 4-μm thickness were used for PAS and H&E staining. IHC staining with goat anti-rat KIM-1 antibody was used to quantify the degree of tubular injury after I/R-induced AKI, following the protocol of Schröppel *et al*. (54). Quantification of tubular regions positive for KIM-1 staining was analyzed in a double-blinded fashion.

Rat PTE cell culture and A/R assays

Immortalized PTE cells from WKY rats were cultured at 37°C in 95% O_2 and 5% CO_2 in DMEM/F-12 (50, 51). To induce anoxia, cells grown on coverslips were placed in an anoxic chamber with 1% oxygen, 5% CO_2, and balanced N_2 at 37°C for 2 hours, followed by reoxygenation for 2 hours. Exogenous rhMG53 or BSA was conjugated with rhodamine by a dye labeling kit (G-Biosciences) and applied to cells immediately after anoxia. After reoxygenation, the cells were used for FITC–annexin V (BD Biosciences) staining and fixed with 4% paraformaldehyde (30 min). Immunofluorescence images were acquired with LSM 780 (Carl Zeiss) confocal microscopy.

MTT cell viability assay

Culture of the KPC-Brca1 pancreatic cancer cells was maintained according to Shakya *et al*. (33, 34). Cisplatin-induced changes in cell viability were determined with MTT assay. Cells were plated at 1000 to 1500 cells per well in a 96-well plate and then treated with the indicated amounts of cisplatin for 48 hours. Then, 20 μl (5 mg/ml in PBS) of MTT (Sigma Chemical Co.) was added to each well. After 4 hours, culture medium was removed, 150 μl of dimethyl sulfoxide was added to dissolve formazan crystals in each well, and absorbance was recorded at 570 nm.

Allograft model

Five-week-old NCR nude mice were implanted subcutaneously in both flanks with 2×10^6 KPC-Brca1 pancreatic cancer cells. After tumors reached 4 to 7 mm in diameter (5 days after implantation), the mice were divided into three groups such that the mean and the variance of the tumor diameters were not significantly different among the groups before treatment. Cisplatin-induced suppression of tumor growth was tested through intraperitoneal administration. Ten minutes before cisplatin administration (6 mg/kg, intraperitoneal), rhMG53 (2 mg/kg) (or an equal volume of saline solution as control) was delivered through tail vein injection. Tumor volume was determined from the orthogonal dimensions (length and width) using the following formula: tumor volume = ½ (length × width^2). According to the IACUC guideline, the animals were euthanized when tumors reached 1.5 cm in diameter. At the end of the experiment, mice were sacrificed, and xeno-grafts were removed and analyzed.

Statistical analysis

All data are expressed as means ± SEM. Comparisons were made by Student's *t* test when comparing two experimental groups and by analysis of variance (ANOVA) for repeated measures. A value of $P < 0.05$ was considered significant. All original data and P values are provided in table S1.

Supplementary Material

Refer to Web version on PubMed Central for supplementary material.

Acknowledgments

We thank the excellent service from Novoprotein Scientific Inc. for providing the scale-up production of rhMG53 protein used in this study and appreciate L. Racusen for providing the HKC-8 cells. We acknowledge the support from the Pathology Core and CMIF Core at The Ohio State University. We also thank R. Cianciolo for help with the KIM-1 IHC studies and H. Ma for reading of the manuscript. **Funding:** This work was supported by NIH grants AR061385, HL069000, and AG028614 to J.M.; U54 CA163111 to T.L.; HL084583, HL083422, and HL114383 to P.J.M.; and U01 DK096927 to B.R. H.Z. was the recipient of an American Heart Association Scientist Development grant.

REFERENCES AND NOTES

1. Saito A, Sato H, Iino N, Takeda T. Molecular mechanisms of receptor-mediated endocytosis in the renal proximal tubular epithelium. J. Biomed. Biotechnol. 2010; 2010:403272. [PubMed: 20011067]
2. Christensen EI, Birn H, Storm T, Weyer K, Nielsen R. Endocytic receptors in the renal proximal tubule. Physiology. 2012; 27:223–236. [PubMed: 22875453]
3. Fuchs TC, Hewitt P. Biomarkers for drug-induced renal damage and nephrotoxicity—An overview for applied toxicology. AAPS J. 2011; 13:615–631. [PubMed: 21969220]
4. Miller RP, Tadagavadi RK, Ramesh G, Reeves WB. Mechanisms of cisplatin nephrotoxicity. Toxins. 2010; 2:2490–2518. [PubMed: 22069563]
5. Linkermann A, Chen G, Dong G, Kunzendorf U, Krautwald S, Dong Z. Regulated cell death in AKI. J. Am. Soc. Nephrol. 2014; 25:2689–2701. [PubMed: 24925726]
6. Eltzschig HK, Eckle T. Ischemia and reperfusion—From mechanism to translation. Nat. Med. 2011; 17:1391–1401. [PubMed: 22064429]
7. Bonventre JV, Yang L. Cellular pathophysiology of ischemic acute kidney injury. J. Clin. Invest. 2011; 121:4210–4221. [PubMed: 22045571]
8. Anders HJ, Muruve DA. The inflammasomes in kidney disease. J. Am. Soc. Nephrol. 2011; 22:1007–1018. [PubMed: 21566058]
9. Leung KC, Tonelli M, James MT. Chronic kidney disease following acute kidney injury—Risk and outcomes. Nat. Rev. Nephrol. 2013; 9:77–85. [PubMed: 23247572]
10. Zhang MZ, Yao B, Yang S, Jiang L, Wang S, Fan X, Yin H, Wong K, Miyazawa T, Chen J, Chang I, Singh A, Harris RC. CSF-1 signaling mediates recovery from acute kidney injury. J. Clin. Invest. 2012; 122:4519–4532. [PubMed: 23143303]
11. McNeil PL, Kirchhausen T. An emergency response team for membrane repair. Nat. Rev. Mol. Cell Biol. 2005; 6:499–505. [PubMed: 15928713]
12. McNeil PL, Steinhardt RA. Plasma membrane disruption: Repair, prevention, adaptation. Annu. Rev. Cell Dev. Biol. 2003; 19:697–731. [PubMed: 14570587]
13. Han R, Bansal D, Miyake K, Muniz VP, Weiss RM, McNeil PL, Campbell KP. Dysferlin-mediated membrane repair protects the heart from stress-induced left ventricular injury. J. Clin. Invest. 2007; 117:1805–1813. [PubMed: 17607357]
14. Bansal D, Miyake K, Vogel SS, Groh S, Chen CC, Williamson R, McNeil PL, Campbell KP. Defective membrane repair in dysferlin-deficient muscular dystrophy. Nature. 2003; 423:168–172. [PubMed: 12736685]
15. Cai C, Masumiya H, Weisleder N, Matsuda N, Nishi M, Hwang M, Ko JK, Lin P, Thornton A, Zhao X, Pan Z, Komazaki S, Brotto M, Takeshima H, Ma J. MG53 nucleates assembly of cell membrane repair machinery. Nat. Cell Biol. 2009; 11:56–64. [PubMed: 19043407]
16. Cao CM, Zhang Y, Weisleder N, Ferrante C, Wang X, Lv F, Song R, Hwang M, Jin L, Guo J, Peng W, Li G, Nishi M, Takeshima H, Ma J, Xiao RP. MG53 constitutes a primary determinant of cardiac ischemic preconditioning. Circulation. 2010; 121:2565–2574. [PubMed: 20516375]

17. Weisleder N, Takizawa N, Lin P, Wang X, Cao C, Zhang Y, Tan T, Ferrante C, Zhu H, Chen PJ, Yan R, Sterling M, Zhao X, Hwang M, Takeshima M, Cai C, Cheng H, Takeshima H, Xiao RP, Ma J. Recombinant MG53 protein modulates therapeutic cell membrane repair in treatment of muscular dystrophy. Sci. Transl. Med. 2012; 4:139ra85.
18. Cai C, Weisleder N, Ko JK, Komazaki S, Sunada Y, Nishi M, Takeshima H, Ma J. Membrane repair defects in muscular dystrophy are linked to altered interaction between MG53, caveolin-3, and dysferlin. J. Biol. Chem. 2009; 284:15894–15902. [PubMed: 19380584]
19. McNeil P. Membrane repair redux: Redox of MG53. Nat. Cell Biol. 2009; 11:7–9. [PubMed: 19122591]
20. Yi JS, Park JS, Ham YM, Nguyen N, Lee NR, Hong J, Kim BW, Lee H, Lee CS, Jeong BC, Song HK, Cho H, Kim YK, Lee JS, Park KS, Shin H, Choi I, Lee SH, Park WJ, Park SY, Choi CS, Lin P, Karunasiri M, Tan T, Duann P, Zhu H, Ma J, Ko YG. MG53-induced IRS-1 ubiquitination negatively regulates skeletal myogenesis and insulin signalling. Nat. Commun. 2013; 4:2354. [PubMed: 23965929]
21. Jia Y, Chen K, Lin P, Lieber G, Nishi M, Yan R, Wang Z, Yao Y, Li Y, Whitson BA, Duann P, Li H, Zhou X, Zhu H, Takeshima H, Hunter JC, McLeod RL, Weisleder N, Zeng C, Ma J. Treatment of acute lung injury by targeting MG53-mediated cell membrane repair. Nat. Commun. 2014; 5:4387. [PubMed: 25034454]
22. Klootwijk ED, Reichold M, Unwin RJ, Kleta R, Warth R, Bockenhauer D. Renal Fanconi syndrome: Taking a proximal look at the nephron. Nephrol. Dial. Transplant. 2014 10.1093/ndt/gfu377.
23. Racusen LC, Monteil C, Sgrignoli A, Lucskay M, Marouillat S, Rhim JG, Morin JP. Cell lines with extended in vitro growth potential from human renal proximal tubule: Characterization, response to inducers, and comparison with established cell lines. J. Lab. Clin. Med. 1997; 129:318–329. [PubMed: 9042817]
24. Ichimura T, Asseldonk EJ, Humphreys BD, Gunaratnam L, Duffield JS, Bonventre JV. Kidney injury molecule–1 is a phosphatidylserine receptor that confers a phagocytic phenotype on epithelial cells. J. Clin. Invest. 2008; 118:1657–1668. [PubMed: 18414680]
25. Lin Q, Chen Y, Lv J, Zhang H, Tang J, Gunaratnam L, Li X, Yang L. Kidney injury molecule-1 expression in IgA nephropathy and its correlation with hypoxia and tubulointerstitial inflammation. Am. J. Physiol. Renal Physiol. 2014; 306:F885–F895. [PubMed: 24523388]
26. Safirstein R, Winston J, Goldstein M, Moel D, Dikman S, Guttenplan J. Cisplatin nephrotoxicity. Am. J. Kidney Dis. 1986; 8:356–367. [PubMed: 3538859]
27. Wensing KU, Ciarimboli G. Saving ears and kidneys from cisplatin. Anticancer Res. 2013; 33:4183–4188. [PubMed: 24122981]
28. Ohndorf UM, Rould MA, He Q, Pabo CO, Lippard SJ. Basis for recognition of cisplatin-modified DNA by high-mobility-group proteins. Nature. 1999; 399:708–712. [PubMed: 10385126]
29. Speelmans G, Staffhorst RW, Versluis K, Reedijk J, de Kruijff B. Cisplatin complexes with phosphatidylserine in membranes. Biochemistry. 1997; 36:10545–10550. [PubMed: 9265635]
30. Jensen M, Bjerring M, Nielsen NC, Nerdal W. Cisplatin interaction with phosphatidylserine bilayer studied by solid-state NMR spectroscopy. J. Biol. Inorg. Chem. 2010; 15:213–223. [PubMed: 19768472]
31. Kramer JH, Misík V, Weglicki WB. Lipid peroxidation-derived free radical production and postischemic myocardial reperfusion injury. Ann. N. Y. Acad. Sci. 1994; 723:180–196. [PubMed: 8030864]
32. Singh AP, Junemann A, Muthuraman A, Jaggi AS, Singh N, Grover K, Dhawan R. Animal models of acute renal failure. Pharmacol. Rep. 2012; 64:31–44. [PubMed: 22580518]
33. Shakya R, Gonda T, Quante M, Salas M, Kim S, Brooks J, Hirsch S, Davies J, Cullo A, Olive K, Wang TC, Szabolcs M, Tycko B, Ludwig T. Hypomethylating therapy in an aggressive stroma-rich model of pancreatic carcinoma. Cancer Res. 2013; 73:885–896. [PubMed: 23204224]
34. Shakya R, Reid LJ, Reczek CR, Cole F, Egli D, Lin CS, deRooij DG, Hirsch S, Ravi K, Hicks JB, Szabolcs M, Jasin M, Baer R, Ludwig T. BRCA1 tumor suppression depends on BRCT phosphoprotein binding, but not its E3 ligase activity. Science. 2011; 334:525–528. [PubMed: 22034435]

35. Sekine M, Monkawa T, Morizane R, Matsuoka K, Taya C, Akita Y, Joh K, Itoh H, Hayashi M, Kikkawa Y, Kohno K, Suzuki A, Yonekawa H. Selective depletion of mouse kidney proximal straight tubule cells causes acute kidney injury. Transgenic Res. 2012; 21:51–62. [PubMed: 21431867]

36. Rennke HG, Patel Y, Venkatachalam MA. Glomerular filtration of proteins: Clearance of anionic, neutral, and cationic horseradish peroxidase in the rat. Kidney Int. 1978; 13:278–288. [PubMed: 651127]

37. Rennke HG, Venkatachalam MA. Glomerular permeability of macromolecules. Effect of molecular configuration on the fractional clearance of uncharged dextran and neutral horseradish peroxidase in the rat. J. Clin. Invest. 1979; 63:713–717. [PubMed: 438331]

38. Shaw A. Update on acute kidney injury after cardiac surgery. J. Thorac. Cardiovasc. Surg. 2012; 143:676–681. [PubMed: 22340031]

39. Cai C, Masumiya H, Weisleder N, Pan Z, Nishi M, Komazaki S, Takeshima H, Ma J. MG53 regulates membrane budding and exocytosis in muscle cells. J. Biol. Chem. 2009; 284:3314–3322. [PubMed: 19029292]

40. Song R, Peng W, Zhang Y, Lv F, Wu HK, Guo J, Cao Y, Pi Y, Zhang X, Jin L, Zhang M, Jiang P, Liu F, Meng S, Cao CM, Xiao RP. Central role of E3 ubiquitin ligase MG53 in insulin resistance and metabolic disorders. Nature. 2013; 494:375–379. [PubMed: 23354051]

41. Nguyen N, Yi JS, Park H, Lee JS, Ko YG. Mitsugumin 53 (MG53) ligase ubiquitinates focal adhesion kinase during skeletal myogenesis. J. Biol. Chem. 2014; 289:3209–3216. [PubMed: 24344130]

42. Ma LL, Zhang FJ, Qian LB, Kong FJ, Sun JF, Zhou C, Peng YN, Xu HJ, Wang WN, Wen CY, Zhu MH, Chen G, Yu LN, Liu XB, Wang JA, Yan M. Hypercholesterolemia blocked sevoflurane-induced cardioprotection against ischemia–reperfusion injury by alteration of the MG53/RISK/GSK3b signaling. Int. J. Cardiol. 2013; 168:3671–3678. [PubMed: 23856444]

43. Yuan H, Niu Y, Liu X, Yang F, Niu W, Fu L. Proteomic analysis of skeletal muscle in insulin-resistant mice: Response to 6-week aerobic exercise. PLOS One. 2013; 8:e53887. [PubMed: 23326526]

44. Xu Y, Ma LL, Zhou C, Zhang FJ, Kong FJ, Wang WN, Qian LB, Wang CC, Liu XB, Yan M, Wang JA. Hypercholesterolemic myocardium is vulnerable to ischemia-reperfusion injury and refractory to sevoflurane-induced protection. PLOS One. 2013; 8:e76652. [PubMed: 24124583]

45. Tamemoto H, Kadowaki T, Tobe K, Yagi T, Sakura H, Hayakawa T, Terauchi Y, Ueki K, Kaburagi Y, Satoh S, Sekihara H, Yoshioka S, Horikoshi H, Furuta Y, Ikawa Y, Kasuga M, Yazaki Y, Aizawa S. Insulin resistance and growth retardation in mice lacking insulin receptor substrate-1. Nature. 1994; 372:182–186. [PubMed: 7969452]

46. Terauchi Y, Iwamoto K, Tamemoto H, Komeda K, Ishii C, Kanazawa Y, Asanuma N, Aizawa T, Akanuma Y, Yasuda K, Kodama T, Tobe K, Yazaki Y, Kadowaki T. Development of non–insulin-dependent diabetes mellitus in the double knockout mice with disruption of insulin receptor substrate-1 and b cell glucokinase genes. Genetic reconstitution of diabetes as a polygenic disease. J. Clin. Invest. 1997; 99:861–866. [PubMed: 9062343]

47. Waddell LB, Lemckert FA, Zheng XF, Tran J, Evesson FJ, Hawkes JM, Lek A, Street NE, Lin P, Clarke NF, Landstrom AP, Ackerman MJ, Weisleder N, Ma J, North KN, Cooper ST. Dysferlin, annexin A1, and mitsugumin 53 are upregulated in muscular dystrophy and localize to longitudinal tubules of the T-system with stretch. J. Neuropathol. Exp. Neurol. 2011; 70:302–313. [PubMed: 21412170]

48. Lin P, Zhu H, Cai C, Wang X, Cao C, Xiao R, Pan Z, Weisleder N, Takeshima H, Ma J. Nonmuscle myosin IIA facilitates vesicle trafficking for MG53-mediated cell membrane repair. FASEB J. 2012; 26:1875–1883. [PubMed: 22253476]

49. Zhu H, Lin P, De G, Choi KH, Takeshima H, Weisleder N, Ma J. Polymerase transcriptase release factor (PTRF) anchors MG53 protein to cell injury site for initiation of membrane repair. J. Biol. Chem. 2011; 286:12820–12824. [PubMed: 21343302]

50. Zeng C, Liu Y, Wang Z, He D, Huang L, Yu P, Zheng S, Jones JE, Asico LD, Hopfer U, Eisner GM, Felder RA, Jose PA. Activation of D_3 dopamine receptor decreases angiotensin II type 1 receptor expression in rat renal proximal tubule cells. Circ. Res. 2006; 99:494–500. [PubMed: 16902178]

51. Parenti A, Cui XL, Hopfer U, Ziche M, Douglas JG. Activation of MAPKs in proximal tubule cells from spontaneously hypertensive and control Wistar-Kyoto rats. Hypertension. 2000; 35:1160–1166. [PubMed: 10818081]

52. Wilson HM, Stewart KN. Glomerular epithelial and mesangial cell culture and characterization. Methods Mol. Biol. 2012; 806:187–201. [PubMed: 22057453]

53. Lieberthal W, Fuhro R, Andry CC, Rennke H, Abernathy VE, Koh JS, Valeri R, Levine JS. Rapamycin impairs recovery from acute renal failure: Role of cell-cycle arrest and apoptosis of tubular cells. Am. J. Physiol. Renal Physiol. 2001; 281:F693–F706. [PubMed: 11553517]

54. Schröppel B, Krüger B, Walsh L, Yeung M, Harris S, Garrison K, Himmelfarb J, Lerner SM, Bromberg JS, Zhang PL, Bonventre JV, Wang Z, Farris AB, Colvin RB, Murphy BT, Vella JP. Tubular expression of KIM-1 does not predict delayed function after transplantation. J. Am. Soc. Nephrol. 2010; 21:536–542. [PubMed: 20019169]

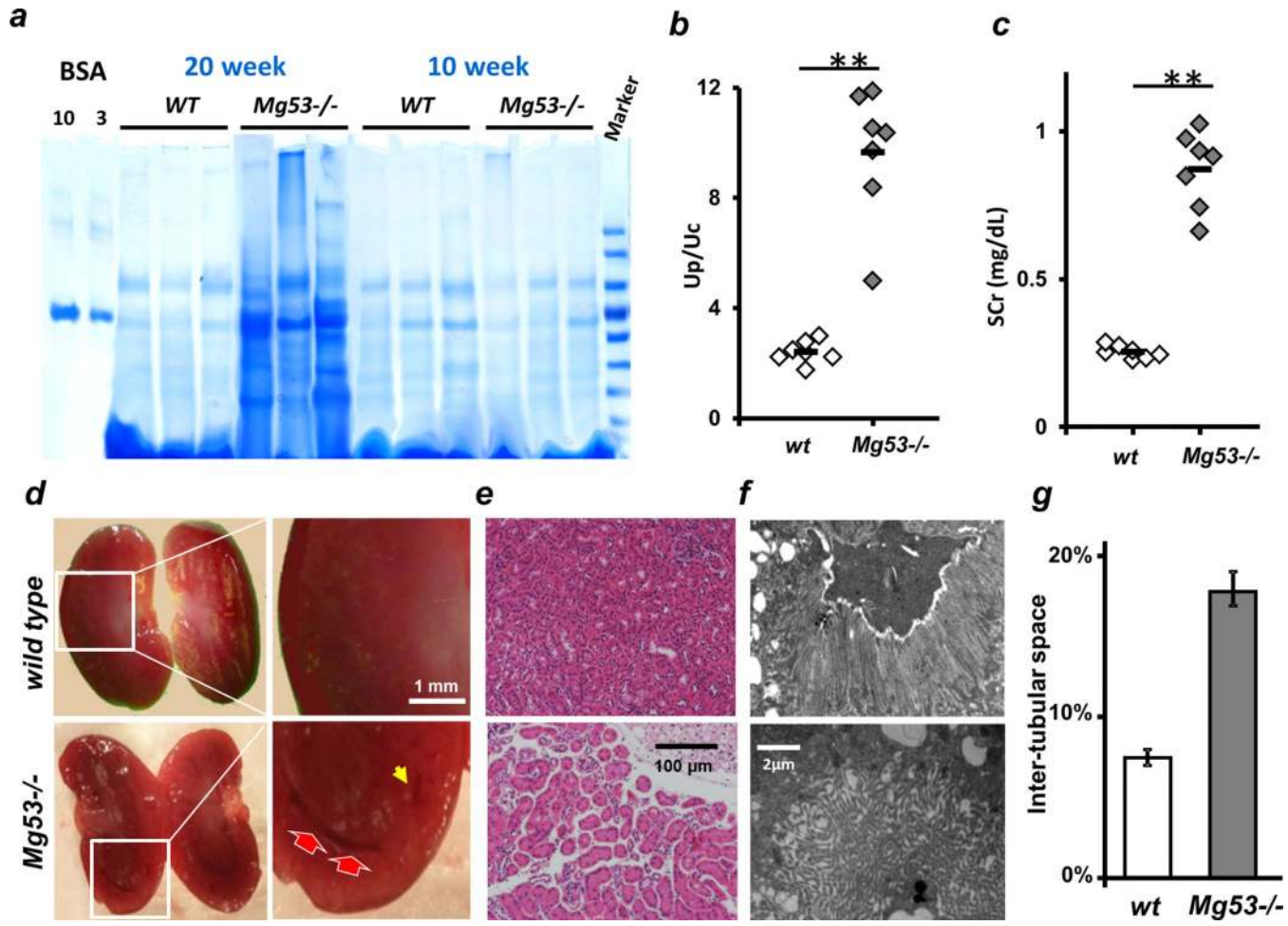

Fig. 1. MG53 deficiency impairs renal function

(**A** and **B**) *Mg53*$^{-/-}$ mice develop proteinuria as they age (20-week versus 10-week ages), as shown by colloidal blue–stained SDS–polyacrylamide gel electrophoresis (SDS-PAGE) of urine (A), and Up/Uc ratios (B). $^{**}P < 0.001$. Bovine serum albumin (BSA) was used as a loading control (10 and 3 μg). (**C**) *Mg53*$^{-/-}$ animals display impaired kidney function with an increase in SCr compared with littermate wild-type (WT) controls ($^{**}P < 0.001$). (**D**) Compared with WT kidney, *Mg53*$^{-/-}$ kidney shows pathology at the inner cortex with pronounced vacuolization (red arrows) and disorganized cisternae (yellow arrow). Scale bar, 1 mm. (**E**) H&E staining shows widening of the interstitial compartment in the *Mg53*$^{-/-}$ kidney. Scale bar, 100 μm. (**F**) Transmission electron micrographs reveal disorganized microvilli and brush border at the apical surface of PTE cells derived from the *Mg53*$^{-/-}$ kidney. Scale bar, 2 μm. (**G**) The intertubular space was ~2.5-fold larger in the *Mg53*$^{-/-}$ kidney than that in the WT kidney (averaged from a total of 12 images; $^{**}P < 0.001$).

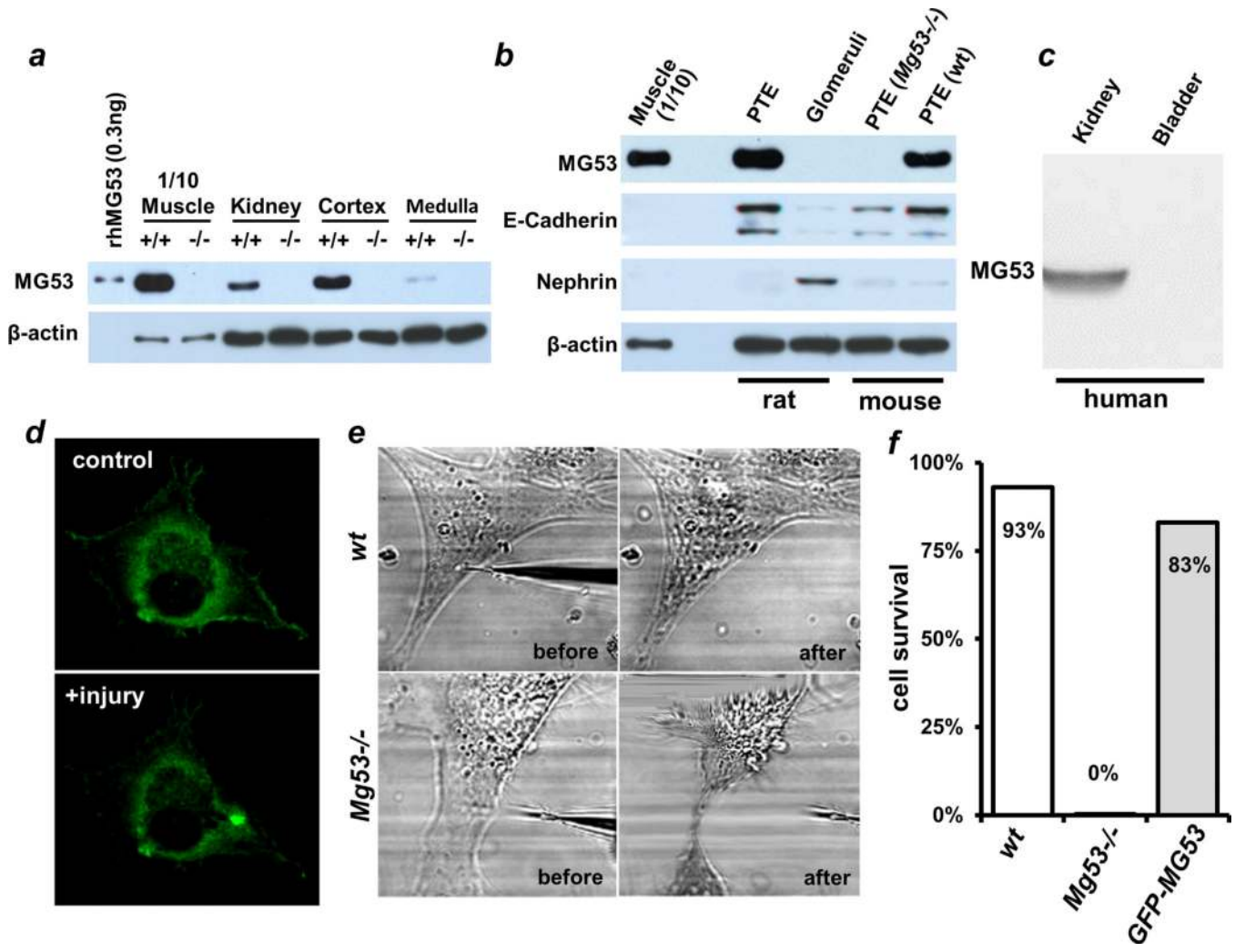

Fig. 2. MG53 mediates membrane repair in proximal tubular epithelial cells

(**A**) Western blot of lysates (50 μg) from total kidney or isolated cortex and medulla derived from WT (+/+) or *Mg53* knockout (−/−) mice. One-tenth of the amount (5 μg) of WT skeletal muscle lysates was used for comparison. Purified rhMG53 was used as a positive control. (**B**) MG53 protein is detected in PTE cells from WT mice and rats, but not in glomeruli isolated from rats or in PTE cells from $Mg53^{-/-}$ mice. The identities of PTE cells or glomeruli were verified by the expression of E-cadherin or nephrin, respectively. (**C**) Total tissue lysates (50 μg) from human kidney and bladder were immunoblotted with anti-MG53 antibody. (**D**) GFP-MG53 expressed in $Mg53^{-/-}$ PTE cells translocates to the area of acute mechanical injury after microelectrode penetration. Scale bar, 10 μm. (**E**) The WT PTE cells survive after acute mechanical injury, whereas the $Mg53^{-/-}$ PTE cells always die within 10 s of micro-electrode penetration. (**F**) GFP-MG53 overexpression rescues survival of $Mg53^{-/-}$ PTE cells after microelectrode-induced membrane damage. *P* values for comparisons with $Mg53^{-/-}$ group are all <0.001.

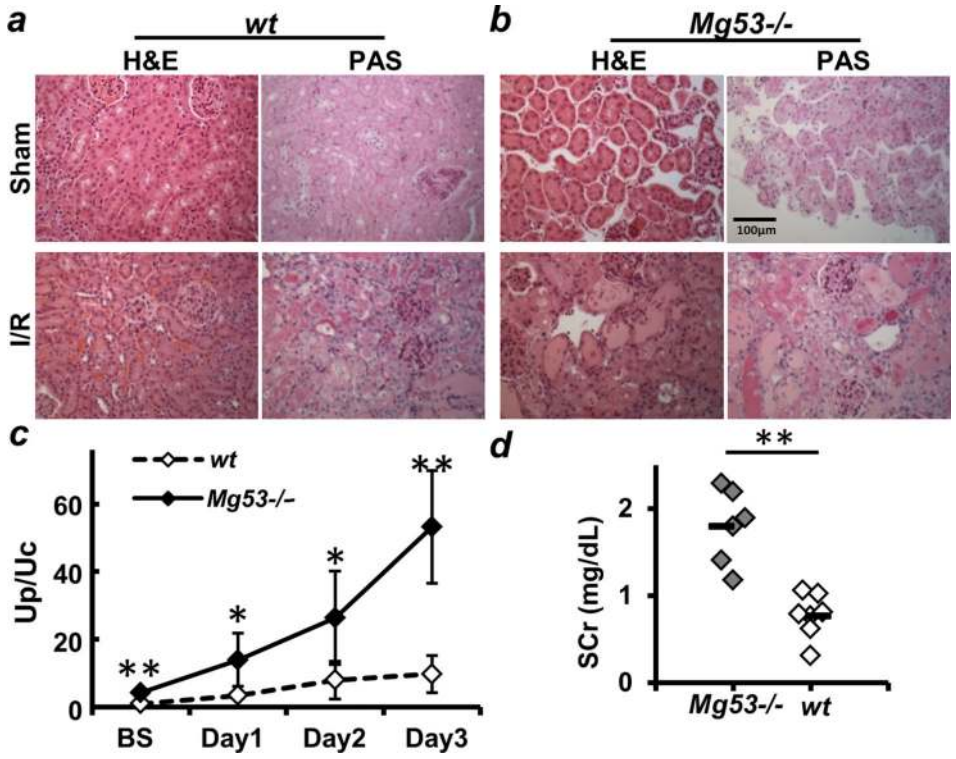

Fig. 3. MG53 deficiency aggravates I/R-induced AKI

(**A** and **B**) H&E and PAS stains were used to evaluate the pathological changes in the kidneys of WT (A) and *Mg53*$^{-/-}$ mice (B) upon sham treatment (top panels) or I/R-induced AKI (bottom panels). Scale bar, 100 μm. *Mg53*$^{-/-}$ kidneys are more susceptible to I/R-induced injury. (**C** and **D**) Time-dependent urinary protein excretion (C) and SCr concentration at 5 days after I/R-induced AKI (D) show significant differences between WT and *Mg53*$^{-/-}$ mice. *$P < 0.01$, **$P < 0.001$.

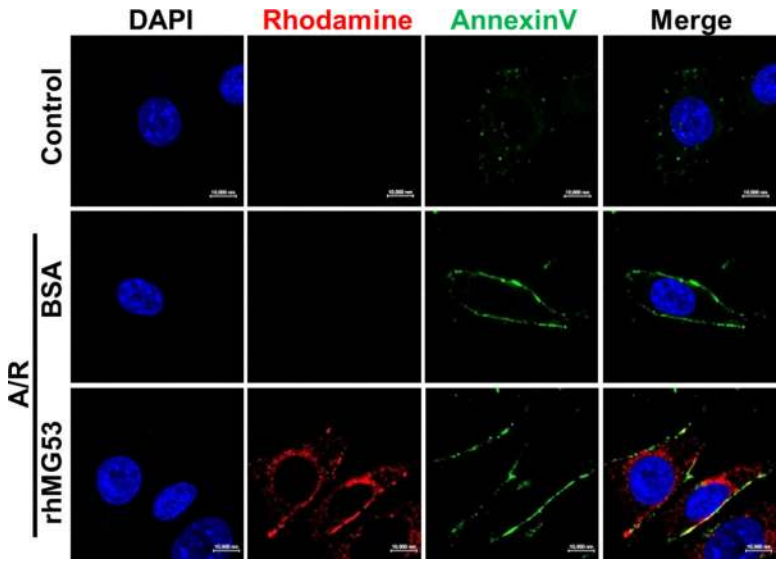

Fig. 4. rhMG53 colocalizes with annexin V at the plasma membrane of PTE cells after A/R injury

PTE cells were treated with rhodamine-labeled rhMG53 (0.1 mg/ml) or rhodamine-labeled BSA (0.1 mg/ml, as control). Immunostaining was performed with fluorescein isothiocyanate (FITC)–annexin V for labeling of PS exposed at the plasma membrane. Control PTE cells are negative for staining with rhMG53 or annexin V. PTE cells exposed to A/R show positive staining with rhMG53 and annexin V (bottom panels). In addition to localization at the plasma membrane (overlapping pattern with annexin V), a portion of rhMG53 could enter the PTE cells after exposure to A/R. As control, cells incubated with BSA (middle panels) showed neither plasma membrane targeting nor intracellular localization of BSA. Scale bar, 10 μm.

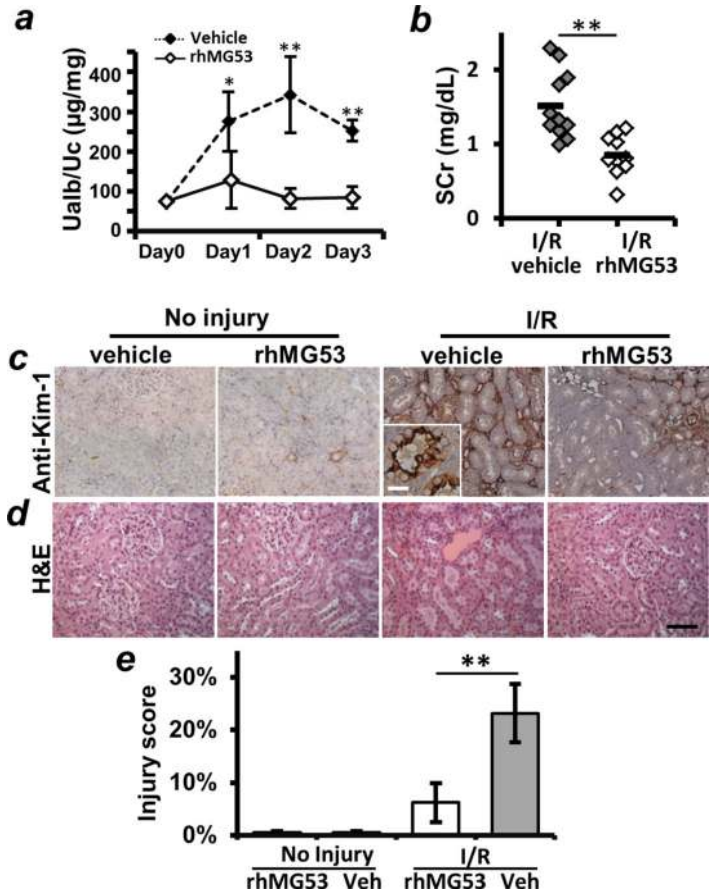

Fig. 5. rhMG53 protein ameliorates I/R-induced AKI in rat model

(**A** and **B**) Kidney function assessed by Ualb/Uc (A) or SCr (B) demonstrates the beneficial effects of rhMG53 in prevention of I/R-induced AKI. (**C**) IHC staining with anti–KIM-1 reveals reduced kidney pathology in rhMG53-treated animals 5 days after I/R injury. (**D**) H&E staining shows that rhMG53 treatment improved kidney histopathology 5 days after I/R-induced AKI. Scale bar, 100 μm. (**E**) Injury scores based on quantitative analysis of KIM-1 [shown in (C)] reveal diminished tubular injury in I/R-injured rats that receive rhMG53 (n = 4 to 9 per group; *P < 0.01, **P < 0.001). Veh, vehicle.

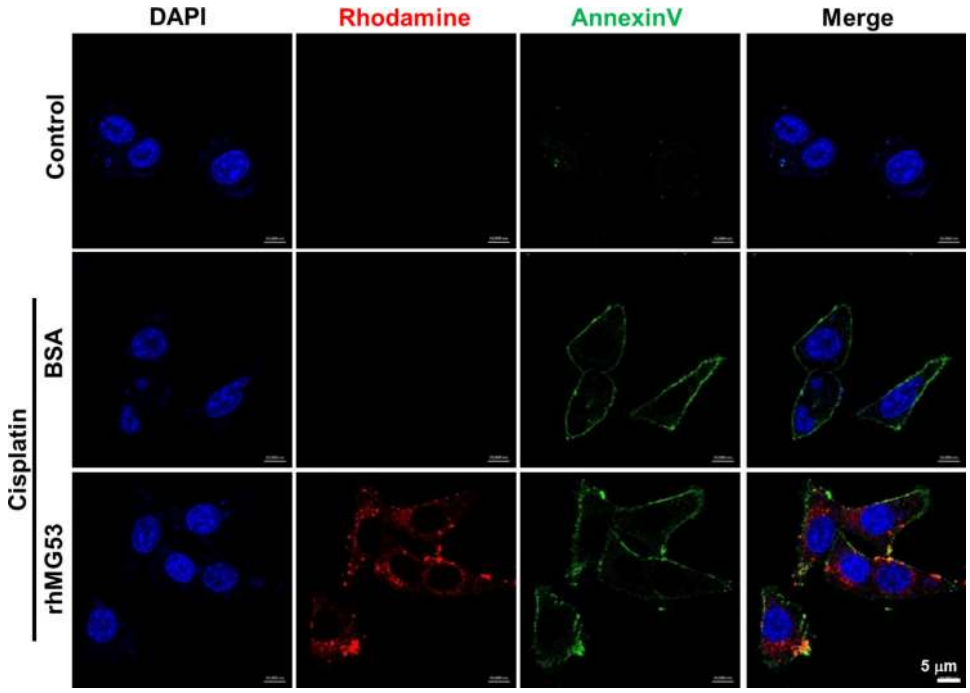

Fig. 6. Cisplatin-induced injury of PTE cells leads to colocalization of rhMG53 and annexin V at the plasma membrane

PTE cells were treated with cisplatin (50 μg/ml) for 3 hours. Rhodamine-labeled rhMG53 (0.1 mg/ml) or rhodamine-labeled BSA (0.1 mg/ml, as control) was then added to the cells. Immunostaining was performed with FITC–annexin V for labeling of exposed PS on the plasma membrane. Control PTE cells are negative for staining with rhMG53 or annexin V. PTE cells exposed to cisplatin show positive staining with rhMG53 and annexin V (bottom panels). Cells incubated with BSA show neither plasma membrane targeting nor intracellular localization of BSA, under control conditions or after cisplatin treatment. Scale bar, 10 μm.

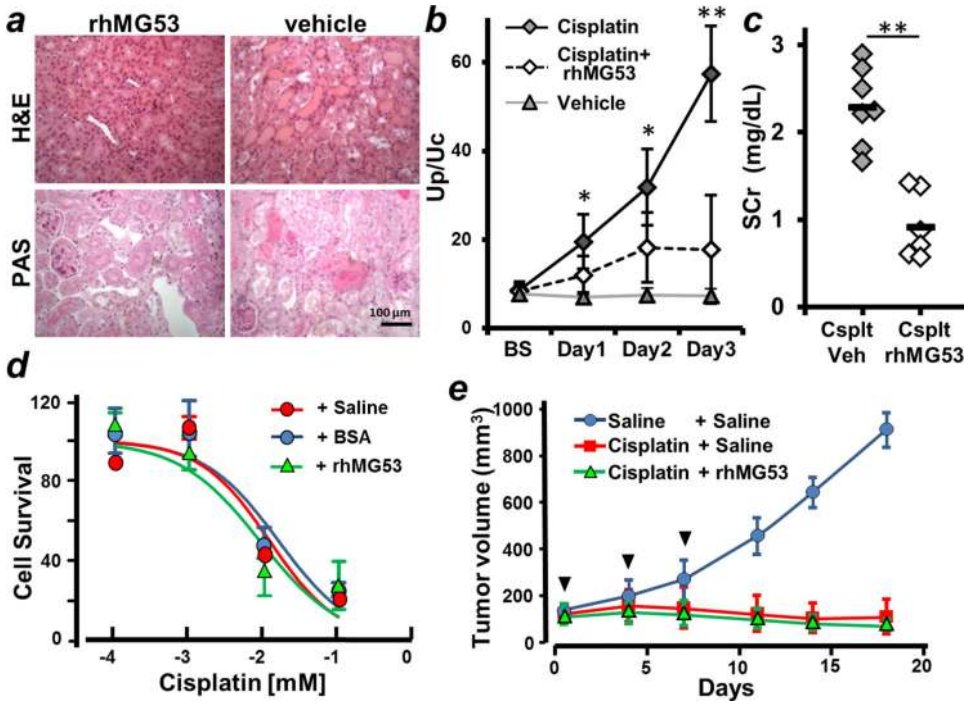

Fig. 7. rhMG53 protects against cisplatin-induced AKI in mice

(**A**) H&E and PAS staining show kidney pathology in WT mice 5 days after cisplatin treatment (30 mg/kg, intraperitoneal). Mice were given one intravenous dose of either rhMG53 (2 mg/kg, left) or vehicle (right) 10 min before cisplatin treatment. Kidney histology showed less severe tubular injury after rhMG53 administration. Scale bar, 100 μm. (**B**) Summary data of urinary protein measurements (Up/Uc) for mice treated with different combinations (vehicle, cisplatin, or cisplatin + rhMG53). (**C**) Mice that received rhMG53 display reduced SCr concentrations at 5 days after cisplatin treatment. *$P < 0.01$, ** $P < 0.001$. (**D**) MTT assay shows that rhMG53 does not alter IC_{50} for cisplatin-induced cell death in murine pancreatic cancer cells (KPC-Brca1). $n = 4$ per group. (**E**) rhMG53 does not alter the efficacy of cisplatin suppression of tumor growth. KPC-Brca1 pancreatic tumor cells were injected subcutaneously into both flanks of nude mice and allowed to grow for 5 days before initiating treatment. Arrows indicate when the mice received injections of cisplatin (6 mg/kg, intraperitoneal) together with rhMG53 (2 mg/kg, intravenous) or saline as vehicle control. Mice demonstrated a similar extent of tumor regression with or without rhMG53 administration ($n = 10$ for each group).

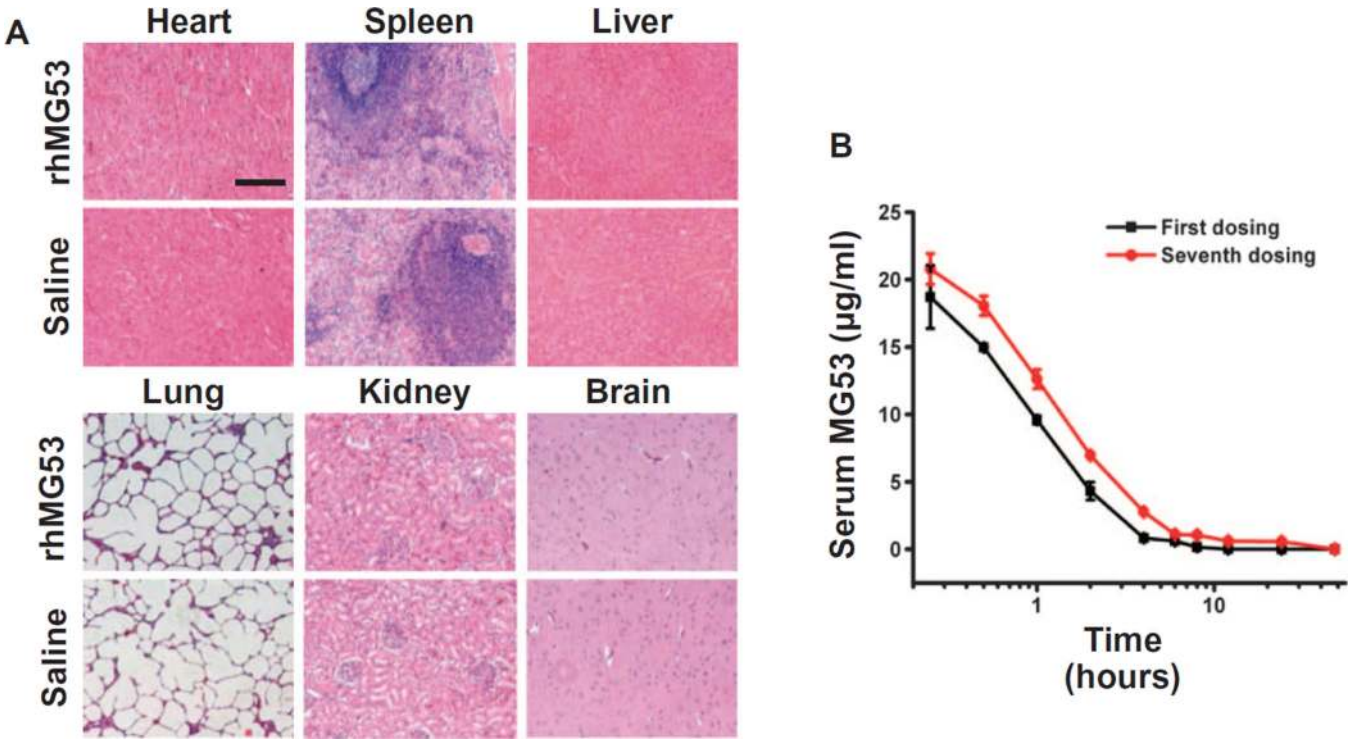

Fig. 8. Repetitive intravenous administration of rhMG53 in beagle dogs

(**A**) rhMG53 (1 mg/kg body weight) was administered to beagle dogs by intravenous injection every other day for a total of seven doses. Histological (H&E staining) analyses did not reveal gross abnormality within major vital organs. Scale bar, 200 μm. (**B**) ELISA determination of serum levels of rhMG53 shows that the pharmacokinetic properties for MG53 remained unchanged between the beginning (first dose) and the end of repeated intravenous administration (seventh dose), with a half-lifetime of ~1.4 hours.